

EVOLUTION FROM THE MAIN SEQUENCE TO THE WHITE DWARF STAGE FOR A $3 M_{\odot}$ STAR

I. MAZZITELLI AND F. D'ANTONA¹

Istituto di Astrofisica Spaziale del C.N.R., Frascati

Received 1985 August 28; accepted 1985 December 10

ABSTRACT

We followed the complete evolution of a Population I $3 M_{\odot}$ initial mass star from the main sequence to the white dwarf (WD) final cooling, by adopting the most reasonably updated input physics for all the evolutionary phases. The main results can be summarized as follows:

i) The mass of a WD remnant of the evolution of an initial $3 M_{\odot}$ star can hardly be smaller than $\sim 0.7 M_{\odot}$, unless some crucial factor is missing from our understanding of stellar evolution. The chemical composition of the WD is stratified: a carbon-rich mantle is superposed on an oxygen-rich core. The WD has a remnant helium envelope of $0.01\text{--}0.02 M_{\odot}$. Overshooting and semiconvection can modify this final picture very little. The mass of the hydrogen layer of the WD can range between the maximum allowed by nuclear burning, which also depends on the exact modalities of sedimentation of CNO elements, and zero, a value which can be attained simply by imposing mass loss rates in the blue consistent with those observed during the planetary nebula (PN) stage.

ii) The hydrogen envelope remnant at the end of the superwind phase largely depends on the residual luminosity of the helium shell, so that in some cases the star can stop its blueward excursion for a time sufficient for the PN to be dispersed before it can be excited.

iii) The evolutionary times of WDs down to invisibility seem to be definitely shorter than the age of the Galactic disk, ranging from 6 to 8×10^9 yr, depending on the surface composition.

Subject headings: stars: evolution — stars: interiors — stars: white dwarfs

I. INTRODUCTION

In spite of a relatively large body of theoretical computations about the evolution of stars in the planetary nebula nucleus (PNN) and white dwarf (WD) phases, several main questions are still subject to debate such as, for instance:

i) Is the mass spectrum for single WDs strongly peaked around $0.58 M_{\odot}$, as suggested by Koester, Schulz, and Weidemann (1979) and stressed by Weidemann and Koester (1983); or is it definitely shallower, indicating a somewhat larger average mass, as would result from "standard" evolution with mass loss of intermediate-mass stars (e.g., Iben and Renzini 1983), as suggested by Shipman (1979) and Shipman and Sass (1980)?

ii) Is the planetary nebula (PN) locus an evolutionary sequence (Schönberner 1981; Schönberner and Weidemann 1981, 1982), or is it rather a convolution of different tracks for different masses in the same range of ages (Renzini 1979)?

iii) What is the internal chemical structure of WDs: pure carbon, an almost homogeneous mixture of carbon and oxygen, or something else?

iv) Are the cooling times of WDs down to the fast Debye phase longer than the age of the Galaxy; or are they much shorter, so that we can suspect a nonnegligible contribution of WDs to the Galactic missing mass (e.g., Liebert 1979; Liebert *et al.* 1979; Liebert 1980)?

We do not even mention other problems, like gravitational settling, interstellar accretion, and so on, since, in our opinion, a better understanding of the physical mechanisms responsible for these phenomena is still necessary for their solution.

In the present paper we try to make a contribution to the understanding of the major questions mentioned above, by discussing the results of a numerical experiment performed by means of Mazzitelli's computer code for stellar evolution. We followed a $3 M_{\odot}$ Population I star from the homogeneous main sequence (MS) to the first major thermal pulse and, through a fast mass loss phase simulating the ejection of a PN, to the contraction at constant luminosity until the degenerate configuration is reached, and finally down through full crystallization and fast Debye cooling. We speak of a "numerical experiment" since we are deeply aware of the many uncertainties still weighing upon the whole stellar evolution theory. This is not, however, too pessimistic a statement, since we are convinced that at least relative indications can be drawn from the present generation of evolutionary models; it is just a warning against abuse in the application of marginal computing results to the interpretation of observational features. This work presents the first results of a series of computations devoted to the evolution of WDs. We will address, in subsequent papers, the following problems:

i) matching the theoretical luminosity function of WDs, derived from the results presented here, with the observational luminosity function, and the role of WDs in the Galactic missing mass problem (D'Antona and Mazzitelli 1986);

ii) the theoretical relation between initial mass and minimum final WD mass, and the chemical composition of WDs for the whole range of Population I initial masses ($1\text{--}7 M_{\odot}$) (Mazzitelli and D'Antona 1986);

iii) full evolution of a $3 M_{\odot}$ star, with "standard" assumptions regarding the mass loss rate, adopting the opacities by Alexander Johnson, and Rypma (1983) which take

¹ Also Osservatorio Astronomico di Roma, Monte Porzio.

into account molecules and grain formation at low T_{eff} (Mazzitelli 1986);

iv) description of the PN phases of evolution.

II. THE COMPUTER CODE

The results reported in the following span all the major phases of a star's life. Although the computer code has been widely tested on several occasions, it is worth recalling its main numerical and physical features to assure the reader that, apart from always possible undetected mistakes, it is reasonably up to date.

The bulk of the code was written during the years 1978–1980 (Mazzitelli 1979; Mazzitelli and Moretti 1980), and minor changes have recently been made. It follows a Raphson-Newton structure, and the mass is the independent variable throughout the star, from the center up to the bottom of the optical atmosphere ($\tau = 2/3$). We found it convenient to avoid using the pressure as an independent variable in a more or less thick “subatmosphere” even if in some cases (e.g., hot WDs) very thin mass steps are required in the external layers. Using a single independent variable has led to a neat and simplified numerical treatment and to the possibility of easily computing chemical evolution and gravitational energy release even very close to the surface. A new zoning for the whole structure is evaluated and applied after each time step, according to the principle that the logarithmic derivatives for all five structural quantities (radius, luminosity, pressure, temperature, and mass) must never exceed given values, fixed by experience and different from region to region. This has led, in the present case, to a minimum number of mesh points, ~ 600 in the main sequence, and ~ 800 – 1000 in the other phases, except for the peak of the thermal pulse, when a maximum of 2500 mesh points was required, to maintain acceptable limits of computer time. Further mesh points are inserted at the boundaries of the convective region after convergence, but no fixed boundary is established for convection during the iterations. Also, the time steps are computed according to maximum allowed logarithm derivatives for the structural quantities, and several other parameters (mass loss, chemistry, integrals over the CNO and 3α luminosities, and so on), but the further requirement has been followed that, when applying to the structural quantities the full corrections computed by solving the matrix of errors and derivatives, convergence has to be reached within no more than three iterations; otherwise the time step must be decreased. In our case we had to compute about 8000 models from MS to WD, but at least the numerical accuracy was ensured on the integration over time, and the low number of iterations helped to keep the computer time fairly acceptable (about 200 hr of CPU on an IBM 370/158). For the computations of the derivatives at the bottom of the optical atmosphere, three gray atmospheres with very small steps in both luminosity and radius ($\delta \ln [L, T_{\text{eff}}] = 0.001$) have been computed for each iteration, avoiding interpolations over fixed, large grids of atmospheres, which can lead to numerical disturbances especially when approaching the surface H ionization with a very thin “subatmosphere” (see § VI).

With regard to the physical inputs, thermodynamics is taken from Magni and Mazzitelli (1979) for pure hydrogen, pure helium, carbon, oxygen, and intermediate mixtures. In partial ionization regions, covolume, van der Waals, Coulomb, and degeneracy effects are taken into account, both as a whole (i.e., for their partial pressures), and for their influence on the internal partition functions and the continuum level. Degeneracy,

relativistic degeneracy, Coulomb, and exchange effects are considered in the regions of full ionization. Crystallization is included following Hansen (1973) and Pollock and Hansen (1973), where the melting parameter is fixed at $\Gamma = 155$.

Pair production has been considered at very high temperatures, for helium, carbon, and oxygen compositions. The effect of metals in partial ionization regions is simulated by assuming carbon (from Fontaine, Graboske, and Van Horn 1977) as an “average metal.” Since the effect of metals in the equation of state is roughly proportional to their mass abundance, this approximation is not so bad as it can seem at first. According to our estimates, for a metal abundance of $Z < 0.04$, the total error in the main thermodynamical quantities due to the use of carbon in place of the correct metallic mixture is hardly larger than $\sim 1\%$, and no equation of state is intrinsically that good.

Nuclear cross sections are from Fowler, Caughlan, and Zimmerman (1975, hereafter FCZ) for the p - p and CNO burning, and from Harris *et al.* (1983, hereafter HFCZ) for the 3α and $^{12}\text{C} + \alpha$ reactions. The nuclear species considered are ^1H , ^3H , ^4He , ^{12}C , ^{14}N , and ^{16}O ; the chemical evolution is carefully followed, allowing each element to relax upon its equilibrium concentration. The screening factors (weak, intermediate, and strong) are from Graboske *et al.* (1973). Plasma, photo, pair, and recombination neutrinos are from Beaudet, Petrosian, and Salpeter (1967). Bremsstrahlung neutrinos are from Lamb and Van Horn (1975), who modified De Zotti's (1972) formula to include functional dependence on the chemical composition. Lamb and Van Horn's formula, however, is far from fitting the asymptotic behaviors for bremsstrahlung neutrinos in the two cases of nondegeneracy and completely relativistic degeneracy, providing values for the neutrino emission rates which are systematically in excess by a factor of 7–9 for a carbon-oxygen composition. For this reason we adopted Lamb and Van Horn's formula, simply divided by a factor of 8, getting a fit always within better than 15% of the asymptotic analytic expressions. It is to be explicitly noted that, since bremsstrahlung neutrinos always represent a nonnegligible fraction (20%–30%) of the total neutrinos in the cores of low- and intermediate-mass stars, their overestimate by a factor 7–9 can easily lead to an overestimate by a factor of 2–3 of the total neutrino fluxes. Radiative opacities are from Cox and Stewart (1970), and conductive opacities from Hubbard and Lampe (1969). We did not include the effects of relativistic degeneracy on the thermal conduction since, in these conditions, our models are already largely isothermal. Superadiabatic convection follows a mixing length scheme, modified by Moss (1968) to estimate the influence of a small magnetic field on the gradients, and reducing to the traditional scheme when the magnetic field intensity is set to zero.

A simple $T(\tau)$ relation (Henyey, Vardya, and Bodenheimer 1965) is adopted all through the gray atmosphere, which is Runge-Kutta integrated in ~ 25 mesh points.

No convective overshooting is explicitly taken into account even if, under some conditions, a discontinuity in the radiative gradient at the edge of the convective core has been found. In any case, a numerical experiment has been carried out, to give an idea of the possible influence of overshooting and semi-convection on the structure of the remnant white dwarf.

The code has been carefully tuned for solar models, leading to the conclusion that the most reasonable choice for the mixing length to fit the observations is, in the framework of our physical inputs, $1/Hp = 2$ (Mazzitelli 1979).

III. FROM THE HOMOGENEOUS MAIN SEQUENCE TO CORE HELIUM BURNING

This evolutionary phase is discussed here for completeness and to perform a few comparisons with computations by other authors as a general check of our evolutionary code. Since we are mainly interested in the behavior of the remnant WD, we will start a more detailed discussion from the latest phases of core helium burning, when a degenerate core first appears.

In Figure 1 we show the complete evolutionary track in the HR diagram, while in Figure 2 the solid line shows the same diagram for only the first part of the evolution for our star ($3 M_{\odot}$, $Y = 0.23$, $Z = 0.02$, mixing length $l/Hp = 2$), from the homogeneous model (A) to the zero-age main sequence (ZAMS; B), to core hydrogen exhaustion (C), to ignition of the hydrogen-burning shell (D), to the fast expansion of the external layers down to the base of the red giant branch (E), up to the top of the red giant branch (F) corresponding to the ignition of helium in the nondegenerate core, down to the position of steady core helium burning (G), and up again to the point where the central helium has been depleted to 1% (H).

It is obviously difficult to make sound quantitative comparisons, even on the MS, without entering into the details of the computer codes. Just as an example, in the present case we realize that an increase in the number of mesh points from 350 to 700 leads to an increase in luminosity in the ZAMS of the order of $\delta \log L/L_{\odot} = 0.05$ (12%). In Figure 2, however, we present the track obtained by Becker (1981) with a version of Iben's evolutionary code, corresponding to $M = 3 M_{\odot}$, $Y = 0.28$, $Z = 0.02$, $l/Hp = 1$, from the MS to the core helium ignition, since this is the most extensive and recent computation for a similar structure. The two sequences are reasonably similar, and the main differences between Becker's and our track are qualitatively in agreement with the expectations, Becker's track being more luminous and hotter in the MS (consistent with a larger helium content) and cooler in the RG phase (consistent with a smaller mixing length value).

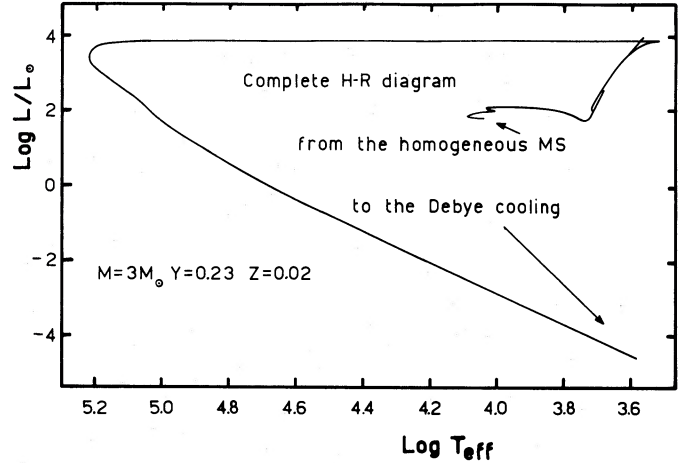


FIG. 1.—Full evolutionary track in the H-R diagram for the $3 M_{\odot}$ star, from the main sequence to the white dwarf stage. The mass is reduced from 3.0 to $0.68 M_{\odot}$ at the top of the asymptotic branch evolution.

One more check on our results is based on a comparison with observations.

Consider the whole red giant region, from point E to the thermal pulse phase. The radius of the star increases from a minimum of $8.5 R_{\odot}$ at E, to about $200 R_{\odot}$ and beyond at the onset of the first thermal pulse. The total time spent in the red giant region for the stars we are considering is about 1.8×10^8 yr, a large fraction of which (1.35×10^8 yr) is spent in the core helium burning phase where according to our models, the radius of the star ranges between 13 and $15 R_{\odot}$. This means that if we select a sample of red giants in a cluster having the proper turnoff age ($3-4 \times 10^8$ yr), about 75% of them are expected to be in the core helium burning phase. Direct comparisons of masses, luminosities, and effective temperatures are difficult due to theoretical and observational problems, apart

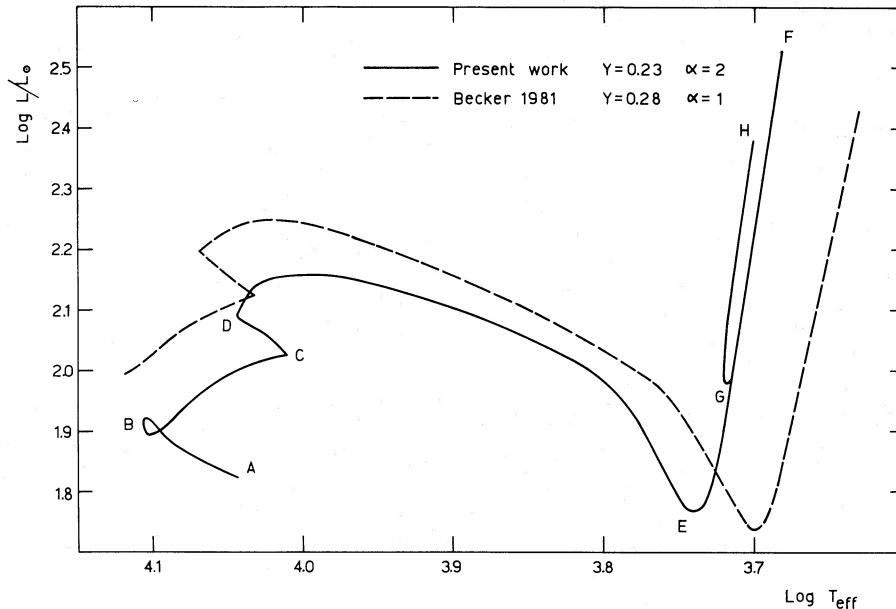


FIG. 2.—Evolutionary track for the $3 M_{\odot}$ star computed here, compared to Becker's (1981). Several relevant points of evolution are indicated: A, homogeneous model; B, zero-age main sequence; C, central hydrogen exhaustion; D, ignition of the hydrogen-burning shell; E, fast expansion of the envelope; F, ignition of helium in the core; G, steady central helium burning; H, central helium reduced to 1%.

from uncertainties in the correlations colors versus BC, T_{eff} , etc. In any case, the results of Coleman (1982) for the observational radii of a number of red giants show that, with a total spread in the radii from 7.6 to 99 R_{\odot} , eight of the nine stars belonging to the Praesepe and Hyades clusters (which are the only ones satisfying the age requirements) have radii in the range 12–16 R_{\odot} , in reasonable agreement with our theoretical expectations.

IV. THE END OF THE CORE HELIUM BURNING PHASE

A small degenerate core, corresponding to the nucleus of the WD to be born, appears at the end of the core helium burning phase. Since the chemical stratification of the WD is relevant for our purposes, let us discuss in some detail the chemical modifications occurring in the core during the central exhaustion of helium. Looking at the behavior of the nuclear cross sections, as a function of the temperature, for the 3α reaction and the $^{12}\text{C} + \alpha$ reaction according to HFCZ, one can see that:

i) In the temperature range in which the central abundance of He drops from 0.1 to 0.01, that is, between ~ 150 and 175×10^6 K, the 3α cross section goes as the 25th power of the temperature.

ii) In the same temperature range the nuclear cross section for the reaction $^{12}\text{C} + \alpha$ is always an order of magnitude or more larger than the 3α cross section.

Point (i) leads to the conclusion that, due to the existence of strong feedback mechanisms in the nondegenerate core, a minor revision in the cross sections would cause a negligible change in the physical structure of the star. Point (ii) has more critical consequences on the chemical composition of the core and deserves further consideration. The ratio between the 3α and the $^{12}\text{C} + \alpha$ reaction rates can be written as

$$48 \langle \sigma_{3\alpha} \rangle X_4^2 \rho / 384 \langle \sigma_{^{12}\text{C}+\alpha} \rangle X_{12} .$$

Given a density of $\sim 3 \times 10^4$ g cm $^{-3}$, the 3α reactions dominate, and ^{12}C accumulates, as long as the helium abundance is larger than a value that, depending on the exact values of temperature and density, ranges in the interval $10\% > X_4 > 3\%$. From this point on, ^{12}C begins to be depleted, and practically all the remaining helium burns via $^{12}\text{C} + \alpha$ reactions, turning into ^{16}O . From a structural point of view, the exact helium abundance at which this turnover takes place is not very relevant since, in any case, it is of interest for only a minor fraction of the helium burning phase. This is not the case for the chemical behavior: in fact, a given fractional abundance by mass of helium, when burning via $^{12}\text{C} + \alpha$ reaction, produces a fractional abundance by mass of ^{16}O four times larger, so that the extra ^{16}O abundance produced during the very last phases of helium burning can range between $\sim 40\%$ and $\sim 10\%$, depending on the turnover point. In other words, for the computation of the physical and chemical characteristics of the final carbon-oxygen core, the use of the correct ratio between the two reactions is determinant.

In our case, the new cross sections (HFCZ) lead to a final oxygen abundance of 75%, whereas a numerical experiment performed with the old cross sections (FCZ) lead to an oxygen abundance lower than 50%.

Another consequence of the preceding discussion, and of the fact that the $^{12}\text{C} + \alpha$ reaction is more favored at lower temperature, is the following: the larger the temperature at exhaustion of helium, the lower the resulting ^{16}O abundance. In our case, the temperature during the central burning phase when

the helium abundance is depleted to 5% is 155×10^6 K, with a final ^{16}O abundance of $\sim 75\%$; in thick shell burning, the corresponding temperature is about 170×10^6 K, with a final ^{16}O abundance of $\sim 40\%$.

In our code no overshooting or semiconvection is explicitly considered, but the behavior of the gradients at the boundary of the convective core was typical of at least the overshooting situation, with a discontinuity in the radiative gradient at the boundary of the core, such that $(\delta \ln T / \delta \ln P)_{\text{rad}} = 0.55$ at the inner edge, and $= 0.32$ at the outer edge when the core helium abundance was depleted to 1%. This is an unstable condition because a small leakage of the convection in the external layers, carrying into the core a large amount of helium, would cause a sudden overgeneration of nuclear energy, with the result of a further increase in the radiative gradient and in the size of the convective core. We frankly admit that the situation could have been different had we properly taken into account semiconvection, but remember that all the currently available recipes for dealing with semiconvection are merely numerical tools for ensuring, by adjusting the chemical composition profile, the equality between radiative and convective gradients, as an *a priori* condition to be fulfilled. In our opinion, this imposed condition deserves further, better physical understanding, in the more general framework of the mechanisms taking place at the border of the convective region.

However, to get an estimate of the possible effects due to large-scale mixing during the last core helium burning phases, we decided to run the code for the two following cases:

A. The size of the convective core was left completely free to move, according to the gradients.

B. The size of the convective core was not allowed to grow, starting from the moment at which the core helium abundance was lower than 5%.

In case A we found that, as soon as the core helium abundance was as low as 0.7%, the convective core with an initial size of 0.24 M_{\odot} began expanding up to a maximum of 0.47 M_{\odot} , increasing the central helium abundance to 42%. The growth of the core was stopped by a sudden expansion of the central regions due to the overgeneration of nuclear energy, and by the consequent absorption of a large amount of gravitational energy, which lowered the energy flux at the boundary of the core, even though at the peak the helium luminosity at the center was as large as 13 times the surface luminosity of the star. From this point on, the rejuvenated star evolved until complete helium exhaustion at the center, without showing any sign of further instability, because the mixing of a large amount of carbon and oxygen resulted in a much smoother gradient profile at the boundary of the convective core.

The thick helium shell phase took over with a slowly increasing efficiency, never producing more than $\sim 65\%$ of the luminosity, until it reached the edge of the former overshooting, where the helium abundance sharply increased and the shell attained its full power, generating $\sim 97\%$ of the surface luminosity.

In case B, the evolution followed a completely different path. The transition between the steady core helium burning and the thick helium shell burning phase was not, in this case, so smooth as was previously found.

When the central helium abundance dropped below $\sim 10^{-4}$, and $\sim 9\%$ of the total luminosity was still produced by the core He burning, the further contraction was no longer able to keep the central nuclear luminosity large enough to maintain a convective core. The abrupt stop of convection and the follow-

ing complete exhaustion of central helium, when a burning shell was not yet ignited, caused a fast overall contraction, leading to the ignition of the shell around the C-O core. At the beginning, the shell was "thin" in the sense discussed by Schwarzschild and Harm (1965). In particular, the two conditions

$$\Delta T/T > 4/\nu$$

and

$$\Delta r/r < 5/2Q,$$

where ν is the power dependence of the nuclear energy generation by the temperature, and $Q = -6$, were fulfilled. In fact, at the temperature of the shell (110×10^6 K), from Figure 3 one can derive $\nu = 38$, so that the two requirements are:

$$\Delta T/T \gtrsim 0.105 \quad \text{and} \quad \Delta r/r \lesssim 0.42.$$

At the minimum shell luminosity, just after the ignition, we evaluate $\Delta T/T \approx 0.23$ and $\Delta r/r \approx 0.35$, so that the condition on the radius for having a "thin" shell was marginally satisfied, whereas the condition on the temperature for having a shell "thick" enough for a thermal runaway to occur was largely fulfilled. As a matter of fact, a series of 11 "micropulses" occurred, until the luminosity profile sharpened enough that the condition on the temperature was no longer fulfilled. Actually, at the end of the last micropulse, $\Delta T/T \approx 0.09$. From this point on, the helium shell became stable against thermal pulsation, until the phase of the major thermal pulses was reached. Figure 3 shows the behavior of the helium and surface luminosities versus the time during the micropulses phase.

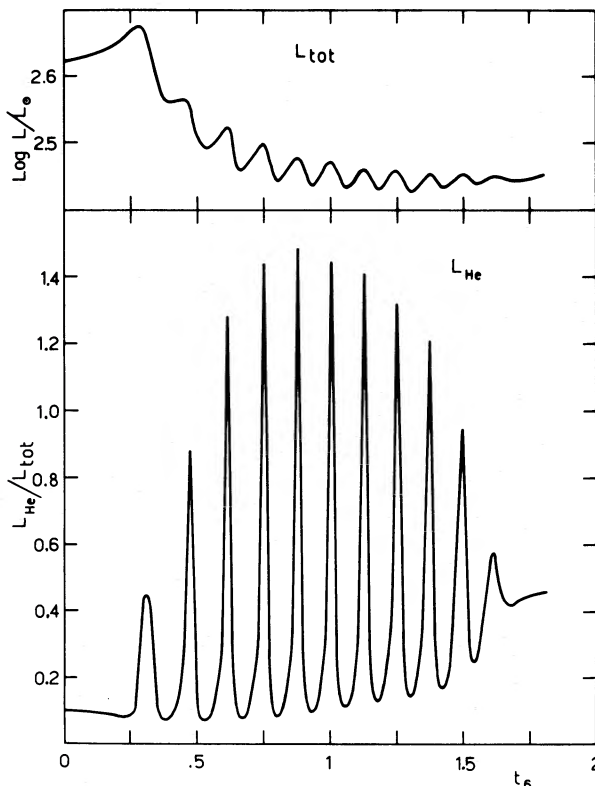


FIG. 3.—Surface luminosity and helium-burning luminosity during the "micropulses" phase following the overall contraction of the carbon-oxygen core at the exhaustion of helium.

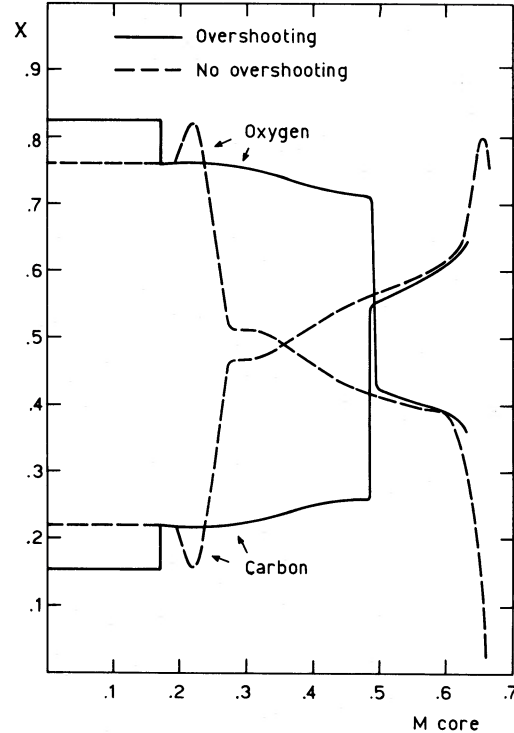


FIG. 4.—Carbon and oxygen abundances in the core of the giant, at the end of the thick shell helium burning phase. The profiles obtained when the convective core boundary is fixed (dashed line) and when overshooting is allowed (solid line) are shown.

The structure of each micropulse presents qualitative resemblances to that of a common thermal pulse, including the temperature inversion and the onset of a convective region at the peak. The maximum helium luminosity at the peak was only $\log(L/L_\odot) = 2.7$, but no other computations exist to exclude that this is the full amplitude of a thermal pulse when the core mass is only $0.25 M_\odot$.

The two cases A and B allow a qualitative estimate of the possible effect of overshooting and semiconvection on the structure of the emerging white dwarf. In Figure 4 are shown the carbon and oxygen profiles versus mass, in the core of the star just before the onset of the first major thermal pulse, for the two cases in which overshooting was respectively allowed (solid lines) and forbidden (dashed lines). As can be seen, overshooting has the effect of increasing the total amount of oxygen in the star ($\sim 67\%$ with overshooting, 55% without). In any case, we get a final stratification of elements such that a carbon-rich ($\sim 60\%$) "mantle" is superposed on an oxygen-rich ($\sim 75\%$) "core." Note also that the last double shell phase almost resets the previous evolution, leading to the same external C-O profiles in each case, and to almost the same total core mass ($M_{\text{WD}} = 0.695 M_\odot$ in case A, and $0.68 M_\odot$ in case B). We conclude that a correct treatment of overshooting and semiconvection can have some influence in determining the chemical profiles in the WD, but very little influence as far as the total mass of the WD is concerned.

The evolution has been followed further for case B. During the helium shell burning phase, the surface luminosity of the star steadily increased and at the turning off of the helium shell, just when the hydrogen shell ignited again, the surface luminosity exceeded $\log(L/L_\odot) = 3.5$ for the first time.

In Figure 5 we show the behavior of the luminosity and of

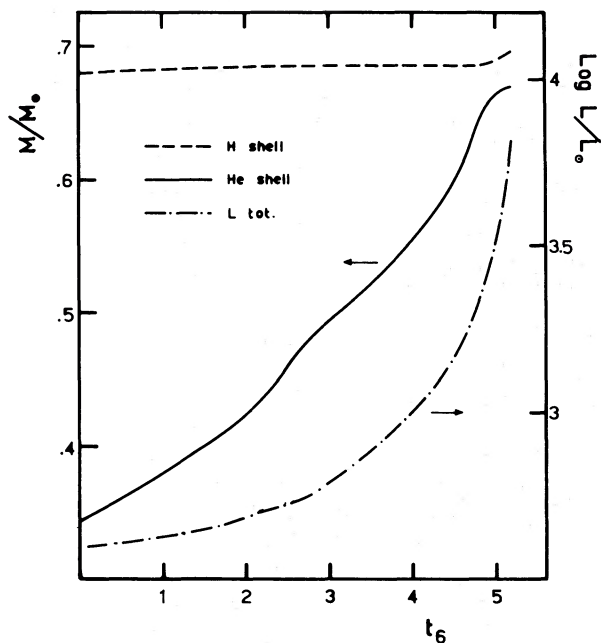


FIG. 5.—Stellar luminosity and mass at the boundary of the helium and hydrogen shells, as function of time, counted from the point at which the helium shell attains 50% of its full power.

the masses at the hydrogen and helium shells versus the time, starting from the point at which the helium shell first reached 50% of its full power, to the onset of the first major thermal pulse. As long as the core of the star is smaller than $0.67 M_{\odot}$, it is very difficult to think of mechanisms responsible for a very fast mass loss phase, since the luminosity of the star is relatively low. It is hard to say if a better input physics could dramatically change this picture. Since the core mass-luminosity correlation for a one-shell burning star is strictly connected to the nuclear cross sections for CNO burning at the thermodynamic conditions existing at the boundaries of a massive degenerate core, and these last conditions are not very sensitive to the opacity, thermodynamics, and so on in the external layers, one could say that, at this point of evolution, any different behavior in the preceding phases due to different physical inputs should have been largely reset. The only way of altering this situation seems to be either to change the cross sections—and by a large factor, otherwise the feedback mechanisms would restore the situation—or to change the surface gravity of the core. The first perspective does not seem very realistic, since the CNO cross sections at the relatively large temperatures of the hydrogen shell ($T > 6 \times 10^7$ K) probably require only minor revisions. Rotation of the degenerate core, on the other hand, could lead to some differences. In particular, one could expect a lower surface gravity for the same core mass, or, alternatively, a larger core mass for the same luminosity. In our opinion this means that, in practice, a star of $3 M_{\odot}$, Population I chemical composition, cannot give rise to a white dwarf having a mass smaller than 0.68 – $0.70 M_{\odot}$. The actual mass may of course be even much larger, depending on the duration of the thermal pulse phase before the ejection of the PN. However, it seems that the thermal pulse phase is not observed at all in many cases, so that an early onset of the superwind, as in our simulation, is probably close to reality (Weidemann 1975; Weidemann and Koester 1983; Weidemann 1984; Iben 1985).

V. THE HELIUM THERMAL PULSE

In the framework of the understanding of the properties of the minimum-mass WD which can reasonably arise from a $3 M_{\odot}$ star, we could have initiated a phase of fast mass loss just at the end of the thick helium shell phase, since both the luminosity and the radius of the star have by then approached the region where, according to observations, planetary nebula ejection might occur. Nevertheless, we decided to postpone the mass loss phase until at least one major thermal pulse had taken place, for two main reasons:

i) the helium zone is nondegenerate, and its contraction can surely contribute to the determination of the evolutionary times of the WD, at least at large luminosities. We felt it better to deal with a helium zone at least partially relaxed on its typical structure during an interpulse phase, which, according to Iben's (1984) computations, should be the case for more than 80% of the WDs. Of course, one thermal pulse is not sufficient for a full relaxation of the helium zone but, as far as the H/He and He/C profiles are concerned, the first pulse is by far the most important one in approaching the equilibrium conditions.

ii) The surface luminosity of the star reaches a maximum during the quiescent helium-burning phase following the thermal pulse and, if the ejection of the planetary nebula is triggered also by the reaching of a critical luminosity, this phase is perhaps the most likely for the planetary nebula event to occur. This can be relevant for the following evolution in the PNN region.

In our models, the luminosity during the interpulse is $\log L/L_{\odot} = 3.9$, about 15% lower than the value given by the Paczyński (1975) relation, and consistent with the behavior found by Becker and Iben (1981), who show that the lower the Y , the lower the interpulse luminosity. The peak power is instead very large ($6.6 \times 10^5 L_{\odot}$) for a first pulse; in this case too, a qualitative agreement with Becker and Iben (1981) is found, in the sense that the peak luminosity for relatively low core masses is larger, the lower Y is and the larger Z is. In any case, the strength of the pulse favors a fair level of relaxation of the helium zone after the pulse.

From the beginning of the pulse to the moment at which the helium luminosity finally drops below 50% of the surface luminosity, the mass at the He/H intershell increases by only $5 \times 10^{-4} M_{\odot}$, so that the final mass of the WD is not altered, and the mass at the He/C interface increases by $5 \times 10^{-3} M_{\odot}$.

At the beginning of the fast mass loss phase, the total mass at the H/He intershell is then $0.68 M_{\odot}$, and the C-O core mass is $0.662 M_{\odot}$, with a helium zone of $0.018 M_{\odot}$. Note that Paczyński's (1975) relation between core mass and helium intershell would require a helium zone of $0.015 M_{\odot}$ for our core mass. It is very likely that the computation of a larger number of thermal pulses would lead to a better agreement, but in any case the difference in mass between our Helium intershell and a fully relaxed one is reasonably small.

VI. THE FAST MASS LOSS PHASE

In deciding when and how to initiate a fast mass loss phase, we had to face a number of problems. First we summarize the major concepts which are currently accepted for the evolution through the PN stage.

i) Renzini (1981) first considered that the very existence of PNs implies that, at a given time, the mass loss rate from asymptotic giant branch (AGB) stars must become much

larger than the normal "wind" rate (Reimers 1975). This "superwind" must be at least several times $10^{-5} M_{\odot} \text{ yr}^{-1}$.

ii) The precise phase during the AGB evolution at which the superwind sets in is also a fundamental parameter for the following evolution, as the helium shell burning is more or less efficient at different stages. Iben (1984) followed numerically a number of cases, showing, for instance, how the complete loss of the hydrogen layer may be achieved if, after the PN ejection, there is the possibility of igniting a final helium shell flash.

iii) It is not clear at all whether PN ejection is a hydrodynamical event or not. The few existing hydrodynamic computations (e.g., Kutter and Sparks 1974) do not consider the resulting behavior of the hydrostatic remnant, whose further evolution to the blue is crucial for the appearance of the PN. Many of the nonhydrodynamical computations—starting from a fundamental paper by Harm and Schwarzschild (1975) and end with Iben (1984)—simulate the dynamical ejection by "scaling" the models before ejection to smaller masses. It is not proven that this procedure is physically meaningful.

In our computations we decided to maintain an "evolutionary continuity" between the starting and final models, avoiding the procedure of scaling the mass. We concentrate on one case of evolution, assuming that the superwind phase begins during the quiescent helium-burning phase immediately following the helium pulse. This stage corresponds to the reaching of maximum surface luminosity and minimum effective temperature, so that the binding energy of the external layers reaches a minimum in this phase. The mass loss rate is approximated by Reimers, (1975) formulation:

$$\dot{M} = -2 \times 10^{-6} \eta (L/10^4 L_{\odot})(R/500 R_{\odot})(M_{\odot}/M) (M_{\odot} \text{ yr}^{-1}).$$

and the parameter η is chosen to assume fixed, very large values. Herman and Habing (1985) find that, for OH-IR masers, which are thought to be in the superwind phase (e.g., Renzini 1984), a modified Reimers formula applies, with

$$\dot{M} = -10^{-5} (L/10^4 L_{\odot})(R/500 R_{\odot})(M_{\odot}/M),$$

so that the observational constraint on η during the superwind is $10\text{--}100\eta$ (Reimers). We used even larger rates, $\eta = 125\text{--}1000$, taking care not to get close to the critical rate for which dynamical effects at the surface begin to be important. This rate can be defined as

$$\dot{M}_d = M_e/t_{\text{ff}},$$

where t_{ff} is the free-fall time at the surface of the star. Adopting the nomenclature of Iben (1984), the blackbody relation for the radius, and a Paczyński-like core mass-luminosity relation scaled on our results, we get

$$\dot{M}_d = 8.5 \times 10^{-12} M_e T_{\text{eff}}^3 (M_h + M_e)^{1/2} (M_h - 0.5)^{-3/4},$$

where M_h is the mass internal to the hydrogen shell and M_e is the mass from the center of the hydrogen shell to the surface. The quantity \dot{M}_d is quite large, as long as M_e is large. Even with $M_e = 2 \times 10^{-3} M_{\odot}$, $\dot{M}_d = 5 \times 10^{-3} M_{\odot} \text{ yr}^{-1}$, so that the rate observed among the infrared OH masers (several times $10^{-4} M_{\odot} \text{ yr}^{-1}$; Knapp *et al.* 1982; Herman and Habing 1985) are not in conflict with the possibility that PN ejection is not a

hydrodynamical event. Vice versa, the thermal equilibrium in the external layers depends on the time scale:

$$t_k = 2 \times 10^7 M^2/LR \text{ yr},$$

where M , L , and R are in solar units, and the critical mass loss rate for being out of thermal equilibrium in the outermost layers is

$$\dot{M}_{\text{th}} = 1.4 \times 10^7 M_e (M_h - 0.5)^{3/2} (M_h + M_e)^{-2} T_{\text{eff}}^{-2}.$$

When $M_e = 2 \times 10^{-3} M_{\odot}$, $\dot{M}_{\text{th}} = 2 \times 10^{-4} M_{\odot} \text{ yr}^{-1}$, so that the gravitational energy in the outermost layers must be properly taken into account for large mass loss rates.

Since we have to get rid of $\sim 2.3 M_{\odot}$, whereas in typical PN ejection of disk stars no more than $0.2\text{--}0.4 M_{\odot}$ is probably ejected, and we want to strip off the external layers in a reasonable time interval, a very large mass loss rate has to be applied, of the order of magnitude of $10^{-4} M_{\odot} \text{ yr}^{-1}$. Although we start with the same efficiency of the helium shell ($L_{\text{tot}} = L_{\text{He}}$), the final phases of mass loss are reached with different contributions of the He shell to the luminosity, as we adopt MLR differing by a factor of ~ 10 . In the first phase of mass loss, the radius increases as the star adjusts itself to the Hayashi track corresponding to smaller and smaller masses, thus also increasing the efficiency of mass loss.

When small envelope masses ($0.2 M_{\odot}$) are reached, the T_{eff} begins to increase. This is the most important stage, as the superwind will finally be quenched when the T_{eff} becomes large enough.

We followed three main cases of evolution:

A. $\eta = 250$ until $M_e = 0.1 M_{\odot}$. Then $\eta = 125$ (A1) and $\eta = 500$ (A2). The case $\eta = 125$ was terminated at $\log T_{\text{eff}} = 3.8$.

B. $\eta = 500$ until $\log T_{\text{eff}} = 3.76$.

C. $\eta = 1000$ until $\log T_{\text{eff}} = 3.76$, then $\eta = 0$.

In cases A2, B, and C the mass loss was stopped when the dynamical effects at the surface began to be of the order of 1%. Pursuing the computations in this case would have resulted in bad models (as hydrostatic equilibrium is assumed), but in any case the quenching of the superwind would have been reached in a very short time due to the fast increase of T_{eff} .

A complete physical discussion of these phases would be very long and, to some extent, beyond the aim of the present paper, so we decided to postpone it to a further work dealing with PN phases. In the following, we only present an overview of the main numerical results, which are also summarized in Figure 6, where the envelope mass is plotted as function of T_{eff} .

In case A the efficiency of the helium shell burning was reduced to $\sim 1\%$ by the time the envelope mass was $\sim 0.1 M_{\odot}$. Also, the thermal equilibrium of the surface layers was preserved, and in the two subsequent cases (A1 and A2) a unique relation was obtained between the T_{eff} and M_e , down to $M_e = 10^{-3} M_{\odot}$, independent of the mass loss rate.

Adopting a larger \dot{M} (cases B and C), the He shell efficiency at $M_e = 0.1 M_{\odot}$ was respectively 30% ($\eta = 1000$) and 10% ($\eta = 500$). As can be seen in Figure 6, the star supports a larger M_e at the same T_{eff} , the larger the He shell luminosity. When mass loss is stopped in the case $\eta = 1000$, the star also stops its evolution toward larger T_{eff} . The surface temperature decreases again, and in $\sim 25,000$ yr the envelope mass is consumed by hydrogen burning, until the star finds itself on the $M_e\text{--}T_{\text{eff}}$ relation of case A. In fact, the He shell contribution to the luminosity decreases to $\sim 1\%$ as in case A.

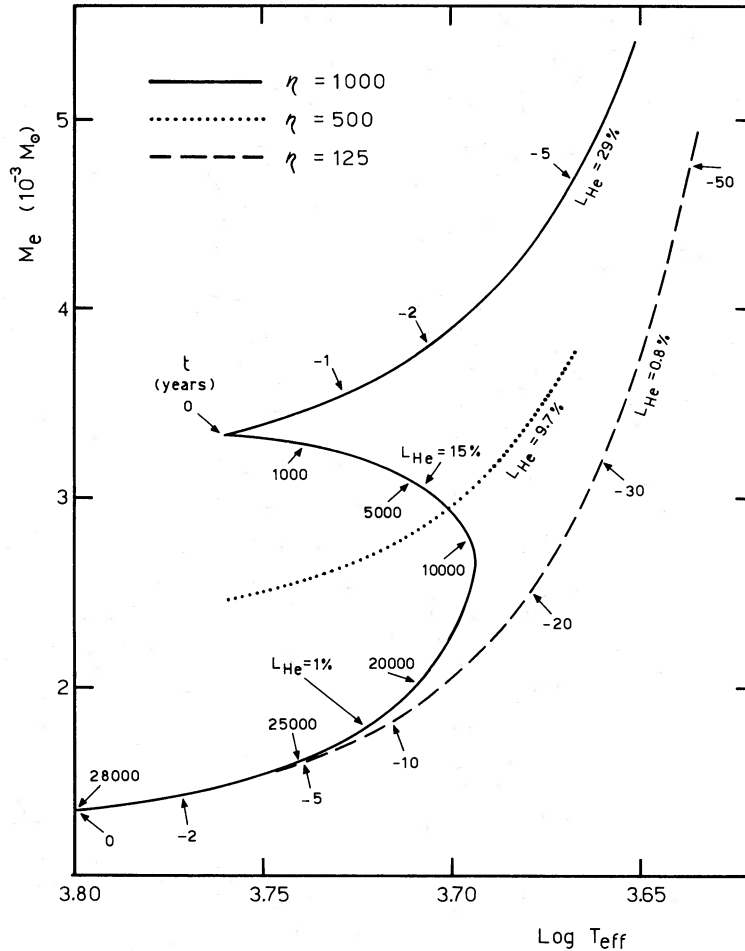


FIG. 6.—The residual hydrogen mass M_e as function of T_{eff} shown during the latest stages of the superwind mass loss phase, in three different cases. In all the sequences, mass loss started at the same point of evolution, but, due to the different rates, different residual helium luminosities are attained. In the sequence $\eta = 1000$, mass loss stops at the point indicated by $t = 0$, and the residual surplus of hydrogen quietly burns in $\sim 25,000$ yr, until the same M_e as in the sequence $\eta = 125$ is reached.

These results seem to indicate that even if the superwind starts at the same precise phase of AGB evolution, the rate itself of mass loss may be determinant for the evolution: a large mass loss rate can leave the star with a massive hydrogen layer, which is then consumed when the superwind ceases, and in the meantime the evolution to the blue is stopped. For any given carbon-oxygen core mass, the possibility of producing an observable PN thus also depends on the mass loss rate during the envelope ejection, and a large mass loss rate may possibly lead to such a long duration in the red that, when the star eventually moves to the blue, the surrounding PN is already dispersed. The result can be seen also from another point of view: for each T_{eff} , different amounts of hydrogen can be supported by the structure, depending on the helium luminosity. As the quenching of the superwind will probably occur at a relatively low T_{eff} , a visible PN will be produced only if this T_{eff} is reached when the helium luminosity is negligible; otherwise the star stops its blueward excursion until all excess hydrogen is burned, in the red.

Our results point toward the existence of a minimum value for M_e at any given T_{eff} (the value corresponding to minimum helium luminosity), so that a star in hydrostatic equilibrium cannot be arbitrarily “peeled” while remaining in the red (as already shown by, e.g., Schönberner 1979), contrary to the

results by Iben (1984), when he uses non evolutionary models. However, our residual envelope masses are definitely larger than the ones found by Schönberner (1979, 1983). At least part of this difference can be due to the different numerical structure of the computer codes. Our code treats the whole star up to the atmosphere in the Raphson Newton scheme, allowing the correct evaluation of surface gravitational energy generation, and avoiding the use of more or less wide grids of “subatmospheres.” Since in these phases even an extremely thin subatmosphere crosses the boundary of the hydrogen ionization, with a near discontinuity of several orders of magnitude in pressure, temperature, and radius at the bottom, we strongly suspect that the use of grids of subatmospheres on the top of an extremely thin H burning shell can introduce non-negligible numerical uncertainties. Other differences can obviously be due to the different input physics, mainly thermodynamics.

VII. THE BLUEWARD EVOLUTION TO THE WHITE DWARF DOMAIN

a) Assumptions

We have stressed that the outcome of the final phases of mass loss depends on several uncertain parameters. We have examined a small range of variations for these parameters, and,

for instance, Iben (1984) has shown that the final He shell flash during the post-AGB phase may lead to the complete loss of the hydrogen envelope in some pre-WDs.

In order to get as complete as possible an understanding of stellar behavior in the WD phase, starting with our pre-PN models, we rely on the following assumptions derived from observations:

i) A class of WDs is hydrogen-lacking: the atmosphere should be composed of practically pure helium: some stars manage to lose their whole hydrogen envelope before they become WDs.

ii) Among the hydrogen atmosphere WDs (DA type), there is no observational evidence about the thickness of the hydrogen layer, although constraints on M_h should be imposed by the consideration that most, if not all, DA WDs pulsate in the ZZ Ceti instability strip: until recently, all pulsation computations agreed in giving an upper limit of $< 10^{-7} M_\odot$ to M_h , in order to have unstable modes of oscillation (e.g., Dolez and Vauclair 1981; Winget, Van Horn, and Hansen 1981), but recently Cox *et al.* (1985) have found instabilities also with $M_h = 6 \times 10^{-5} M_\odot$. A further possible constraint can be used: there is an indication that mixing of the hydrogen layer with the helium beneath has taken place in some cool WDs (6000–7000 K) (Wehrse and Liebert 1980; Liebert 1979; Sion 1979). Using recent good-quality data, Greenstein (1986) again finds that the DAs are only 20% of the total number of very cool WDs. This constrains M_e to 10^{-10} to $10^{-7} M_\odot$, so that the hydrogen convection may penetrate down to the bottom of the hydrogen envelope (e.g., D'Antona and Mazzitelli 1979, here after DM).

Consequently, the remaining hydrogen mass is confined between the maximum evolutionary mass (for which burning may still go on) and $M_e \approx 10^{-10} M_\odot$.

iii) Gravitational settling of heavy elements acts in WDs, so that their atmospheres are almost devoid of metals and are completely devoid of helium, even if the pre-WD had a Population I composition. Even in the helium atmosphere WDs showing carbon lines or bands, the derived abundance of carbon is not very large (Zeidler 1984). For DA WDs assumed to have their evolutionary remnant envelope, the modalities of hydrogen-burning will depend on the modalities for the occurrence of gravitational settling of CNO at the inner interface with the helium envelope.

According to these observations, we computed the following cases of evolution:

A. Complete evolution without mass loss maintaining the outer layers' chemical composition at $Y = 0.23$, $Z = 0.02$.

B. Starting from sequence A, we artificially forced depletion of heavy elements in the whole hydrogen envelope, leaving $Y = 0.23$ and $Z = 10^{-5}$. Depletion was forced at $\log T_{\text{eff}} = 5.0$, on a time span of ~ 2000 yr.

C. Mass loss at constant rate of $10^{-8} M_\odot \text{ yr}^{-1}$ was resumed in sequence A, at large luminosities and $\log T_{\text{eff}} = 4.0$, and maintained until the helium-rich layers appeared at the surface, about at $\log (L/L_\odot) = 2.0$. The metal content was left at $Z = 0.02$.

D. The metal content of sequence C was reduced to $Z = 10^{-5}$.

E. A hydrogen layer of $M_H = 10^{-7} M_\odot$ ($Y = 0$, $Z = 10^{-5}$) was left on the WD.

It is clear that sequences A and C are not consistent with the observational evidence that the metal content is drastically

reduced in all WD spectra. Further, sequence B was obtained by an artificial reduction of the metal content. Iben and McDonald (1985) have recently shown that complete metal depletion takes a time span of $\sim 10^6$ yr during the phases in which hydrogen-burning by CNO is still important: therefore, in sequence B, we may possibly be left with too much hydrogen.

Nevertheless, all these tracks will give us important information concerning at least the differential behavior of the physics, and thus of the WD evolutionary times, following different assumptions.

Sequences D and E are probably the most realistic, so they will be used for comparisons with the observations. In Table 1 we summarize the evolutionary times and effective and central temperatures for each sequence, as function of the total luminosity. Note that the starting point of the evolutionary times is chosen to be $t = 5.398E + 08$ for all the sequences. This leads to some insignificant differences at the starting luminosity, which are totally forgotten when the times become longer.

In Table 2 we give the surface abundances of hydrogen and CNO during the later phases of evolution with constant mass loss, through which the WD of sequence C becomes totally deprived of hydrogen.

b) *The Overall Behavior of WDs at $\log (L/L_\odot) < -3.0$*

Iben and Tutukov (1984, here after IT), by pursuing the first "evolutionary" computations of WDs "cooling," gave a fundamental description of the physical processes acting during the WD phase, starting from the turnover of the effective temperature at high luminosity, down to $\log (L/L_\odot) = -5$. We follow their presentation for our sequence A, giving in Figure 7 the evolution of the partial luminosity outputs due to the contribution of hydrogen burning, of helium burning, neutrino losses, and gravitational energy release plus thermal energy release, as a function of the surface luminosity. The central and maximum temperatures and the ages are also given.

Let us discuss first the main features of the WD evolution down to $\log (L/L_\odot) = -3.0$. At $\log (L/L_\odot) = 3$ there is a sudden reduction of CNO burning (see also IT), and gravitational energy release becomes the dominant source of luminosity. The helium luminosity for our track never exceeds 20% and sharply declines below $\log (L/L_\odot) = 2.0$. Between $2.0 > \log (L/L_\odot) > -1.0$, the strong neutrino losses are balanced by the gravitational energy release which occurs mainly in the core. At $\log (L/L_\odot) = -0.8$, the p - p luminosity becomes larger than the CNO luminosity. At $-2 > \log (L/L_\odot) > -3$, p - p burning again provides 20% of the total luminosity output. IT evolution is qualitatively similar, but for the facts that: (1) CNO burning ceases to be important at larger luminosities than in our case, as their models have $Z = 0.001$, compared to our $Z = 0.02$. (2) For the same reason, their hydrogen envelope mass is slightly larger than ours and, very likely, this is the reason why, at $\log (L/L_\odot) < -3.0$ p - p burning becomes the dominant source of luminosity (see also DM for the large dependence of the nuclear output on M_e at low luminosity). A similar result, smaller remnant M_H and consequent lower relative importance of p - p burning at low luminosity, is found by Koester and Schönberner (1986), who adopt $Z = 0.021$ in similar computations.

Apart from the fact that there is no source of nuclear energy, sequences C, D, and E all behave in the same qualitative way as sequence A. The nuclear luminosity of sequence A never exceeding 20%, there is also no appreciable difference in the

TABLE 1
 WHITE DWARF EVOLUTIONARY TIMES

| logL/L _⊙ | sequence A | | | sequence B | | | sequence C | | | sequence D | | | sequence E | | |
|---------------------|------------|---------------------|-------------------|------------|---------------------|-------------------|------------|---------------------|-------------------|------------|---------------------|-------------------|------------|---------------------|-------------------|
| | age | logT _{eff} | logT _c |
| 2.0 | 8.26e+04 | 5.03 | 7.97 | 0.0 | 5.02 | 7.98 | 2.29e+03 | 5.08 | 7.98 | | | | 4.86e+03 | 5.07 | 7.98 |
| 1.6 | 2.06e+05 | 4.98 | 7.94 | 9.70e+04 | 4.97 | 7.96 | 8.80e+04 | 5.01 | 7.96 | | | | 8.30e+04 | 5.00 | 7.96 |
| 1.4 | 2.89 | 4.94 | 7.93 | 1.78e+05 | 4.94 | 7.94 | 1.67e+05 | 4.97 | 7.94 | | | | 1.68e+05 | 4.97 | 7.94 |
| 1.2 | 3.70 | 4.91 | 7.91 | 2.76 | 4.91 | 7.92 | 2.66 | 4.94 | 7.92 | | | | 2.66 | 4.93 | 7.92 |
| 1.0 | 4.85 | 4.87 | 7.89 | 3.88 | 4.87 | 7.90 | 3.71 | 4.90 | 7.90 | | | | 3.79 | 4.89 | 7.90 |
| 0.8 | 6.50 | 4.83 | 7.87 | 5.65 | 4.83 | 7.87 | 5.28 | 4.86 | 7.88 | | | | 5.20 | 4.86 | 7.88 |
| 0.6 | 8.81 | 4.79 | 7.85 | 8.10 | 4.79 | 7.85 | 7.43 | 4.82 | 7.86 | 7.40e+05 | 4.82 | 7.85 | 7.40 | 4.81 | 7.85 |
| 0.4 | 1.20e+06 | 4.75 | 7.82 | 1.18e+06 | 4.75 | 7.82 | 1.04e+06 | 4.77 | 7.83 | 1.04e+06 | 4.78 | 7.83 | 1.05e+06 | 4.77 | 7.83 |
| 0.2 | 1.63 | 4.71 | 7.80 | 1.73 | 4.71 | 7.80 | 1.45 | 4.73 | 7.81 | 1.45 | 4.73 | 7.81 | 1.45 | 4.73 | 7.81 |
| 0.0 | 2.18 | 4.67 | 7.78 | 2.58 | 4.67 | 7.77 | 2.00 | 4.69 | 7.79 | 2.00 | 4.69 | 7.79 | 2.00 | 4.69 | 7.79 |
| -0.2 | 2.89 | 4.62 | 7.76 | 3.80 | 4.63 | 7.73 | 2.70 | 4.64 | 7.77 | 2.70 | 4.64 | 7.77 | 2.72 | 4.64 | 7.77 |
| -0.4 | 3.80 | 4.58 | 7.74 | 6.40 | 4.58 | 7.68 | 3.57 | 4.60 | 7.74 | 3.57 | 4.60 | 7.74 | 3.57 | 4.60 | 7.74 |
| -0.6 | 5.15 | 4.53 | 7.71 | 1.28e+07 | 4.53 | 7.59 | 4.80 | 4.55 | 7.71 | 4.80 | 4.55 | 7.71 | 4.89 | 4.55 | 7.71 |
| -0.8 | 7.39 | 4.48 | 7.67 | 2.56 | 4.50 | 7.50 | 6.90 | 4.50 | 7.68 | 6.90 | 4.50 | 7.68 | 6.96 | 4.50 | 7.68 |
| -1.0 | 1.20e+07 | 4.43 | 7.61 | 4.42 | 4.45 | 7.43 | 1.08e+07 | 4.46 | 7.62 | 1.09e+07 | 4.46 | 7.62 | 1.12e+07 | 4.46 | 7.61 |
| -1.2 | 2.04 | 4.39 | 7.54 | 6.77 | 4.40 | 7.37 | 1.83 | 4.41 | 7.55 | 1.84 | 4.41 | 7.55 | 1.87 | 4.41 | 7.54 |
| -1.4 | 3.80 | 4.35 | 7.45 | 1.03e+08 | 4.35 | 7.30 | 3.35 | 4.36 | 7.47 | 3.40 | 4.36 | 7.46 | 3.36 | 4.36 | 7.46 |
| -1.6 | 6.70 | 4.30 | 7.37 | 1.52 | 4.31 | 7.24 | 5.86 | 4.32 | 7.38 | 6.00 | 4.32 | 7.37 | 6.00 | 4.31 | 7.37 |
| -1.8 | 1.14e+08 | 4.25 | 7.28 | 2.12 | 4.26 | 7.18 | 9.70 | 4.27 | 7.29 | 9.80 | 4.27 | 7.29 | 9.80 | 4.26 | 7.28 |
| -2.0 | 1.79 | 4.20 | 7.20 | 3.00 | 4.20 | 7.11 | 1.51e+08 | 4.22 | 7.21 | 1.53e+08 | 4.22 | 7.20 | 1.55e+08 | 4.21 | 7.20 |
| -2.2 | 2.65 | 4.16 | 7.12 | 4.00 | 4.16 | 7.05 | 2.22 | 4.17 | 7.13 | 2.24 | 4.17 | 7.12 | 2.20 | 4.17 | 7.12 |
| -2.4 | 3.74 | 4.11 | 7.05 | 5.30 | 4.11 | 6.99 | 3.11 | 4.12 | 7.05 | 3.11 | 4.12 | 7.04 | 3.13 | 4.12 | 7.04 |
| -2.6 | 5.10 | 4.06 | 6.97 | 6.90 | 4.06 | 6.93 | 4.26 | 4.07 | 6.97 | 4.22 | 4.07 | 6.96 | 4.20 | 4.07 | 6.96 |
| -2.8 | 6.90 | 4.00 | 6.90 | 9.00 | 4.01 | 6.87 | 5.77 | 4.02 | 6.89 | 5.77 | 4.02 | 6.88 | 5.76 | 4.02 | 6.88 |
| -3.0 | 9.18e+08 | 3.96 | 6.83 | 1.16e+09 | 3.97 | 6.80 | 7.87e+08 | 3.97 | 6.81 | 7.94e+08 | 3.97 | 6.80 | 7.80e+08 | 3.97 | 6.80 |
| -3.2 | 1.22e+09 | 3.92 | 6.76 | 1.45 | 3.92 | 6.74 | 1.05e+09 | 3.93 | 6.74 | 1.12e+09 | 3.93 | 6.71 | 1.05e+09 | 3.92 | 6.73 |
| -3.4 | 1.68 | 3.87 | 6.69 | 1.96 | 3.87 | 6.67 | 1.52 | 3.87 | 6.66 | 1.65 | 3.88 | 6.60 | 1.51 | 3.87 | 6.65 |
| -3.6 | 2.33 | 3.82 | 6.61 | 2.58 | 3.82 | 6.60 | 2.07 | 3.83 | 6.58 | 2.42 | 3.83 | 6.46 | 2.05 | 3.82 | 6.57 |
| -3.8 | 3.06 | 3.77 | 6.54 | 3.34 | 3.77 | 6.52 | 2.85 | 3.78 | 6.49 | 3.17 | 3.78 | 6.33 | 2.80 | 3.77 | 6.49 |
| -4.0 | 4.22 | 3.72 | 6.46 | 4.95 | 3.72 | 6.40 | 3.93 | 3.73 | 6.39 | 3.80 | 3.72 | 6.20 | 4.29 | 3.72 | 6.34 |
| -4.2 | 5.98 | 3.67 | 6.33 | 6.70 | 3.67 | 6.20 | 5.11 | 3.68 | 6.28 | 4.30 | 3.68 | 6.09 | 5.64 | 3.68 | 6.14 |
| -4.4 | 7.80 | 3.61 | 6.18 | | | | 6.33 | 3.63 | 6.16 | 4.90 | 3.62 | 5.92 | 6.47 | 3.62 | 5.95 |
| -4.6 | 9.29 | 3.57 | 6.03 | | | | 7.57 | 3.58 | 6.02 | 5.30 | 3.56 | 5.72 | 6.75 | 3.56 | 5.85 |
| -4.8 | 1.02e+10 | 3.51 | 5.86 | | | | 8.57 | 3.52 | 5.84 | | | | 7.00 | 3.51 | 5.77 |

evolutionary times of all the sequences down to $\log(L/L_{\odot}) = -3.0$.

An instructive comparison can be made between sequences A and B. In Figure 8 we show the percentages of power supplied by the different sources for both sequences A and B. At $\log(L/L_{\odot}) = 3.$, where depletion of metals is forced, the CNO luminosity drops to zero in sequence B, and the gravitational energy release has to become larger than in case A, in order to balance the neutrino losses. At $\log(L/L_{\odot}) = -1.0$, neutrinos became less important, and the p - p luminosity takes over, rea-

ching as much as 70% of the total. Nuclear burning is relevant down to -3.0 . The H-burning output is important for the determination of the total evolutionary times in the range $-0.5 > \log(L/L_{\odot}) > -2.5$, both for our sequence B and for the IT hydrogen sequence. In this region the times become up to a factor of 3.3 longer than for the helium sequences, or even for sequence A in which nuclear burning is never dominant (Fig. 9).

The T_{eff} range in which the maximum difference in t_{ev} occurs is $4.5 > \log T_{\text{eff}} > 4.3$. In the assumption that DAs are

 TABLE 2
 LOSS OF THE HYDROGEN ENVELOPE IN SEQUENCE C

| Age (yr) | $M_{\text{H}} (M_{\odot})$ | $\log(L/L_{\odot})$ | $\log T_{\text{eff}}$ | X_{H} | $X_{^{12}\text{C}} (\times 10^{-4})$ | $X_{^{14}\text{N}} (\times 10^{-2})$ | $X_{^{16}\text{O}} (\times 10^{-4})$ |
|------------|----------------------------|---------------------|-----------------------|----------------|--------------------------------------|--------------------------------------|--------------------------------------|
| 0.0..... | 5.39E - 04 | 2.311 | 5.072 | 0.7457 | 0.38 | 0.39 | 77.0 |
| 3350..... | 3.55E - 04 | 2.271 | 5.069 | 0.7455 | 0.367 | 0.397 | 76.8 |
| 6580..... | 3.27E - 04 | 2.212 | 5.064 | 0.7425 | 0.401 | 0.446 | 71.2 |
| 12300..... | 3.10E - 04 | 2.132 | 5.067 | 0.6413 | 0.830 | 0.910 | 17.3 |
| 14900..... | 2.85E - 04 | 2.103 | 5.074 | 0.4571 | 0.950 | 1.30 | 3.54 |
| 16400..... | 2.70E - 04 | 2.086 | 5.078 | 0.3142 | 0.968 | 1.04 | 2.00 |
| 18400..... | 2.67E - 04 | 2.058 | 5.072 | 0.1415 | 0.996 | 1.05 | 1.50 |
| 20600..... | 2.64E - 04 | 2.044 | 5.079 | 0.0458 | 1.05 | 1.05 | 1.33 |
| 33700..... | 1.36E - 04 | 1.931 | 5.063 | 2.33E - 06 | 2.73 | 1.03 | 1.03 |
| 45900..... | 3.4E - 06 | 1.851 | 5.049 | 1.51E - 12 | 2.88 | 1.03 | 1.00 |
| 49200..... | 0.0E - 06 | 1.830 | 5.046 | 0.0 | 2.89 | 1.03 | 1.00 |

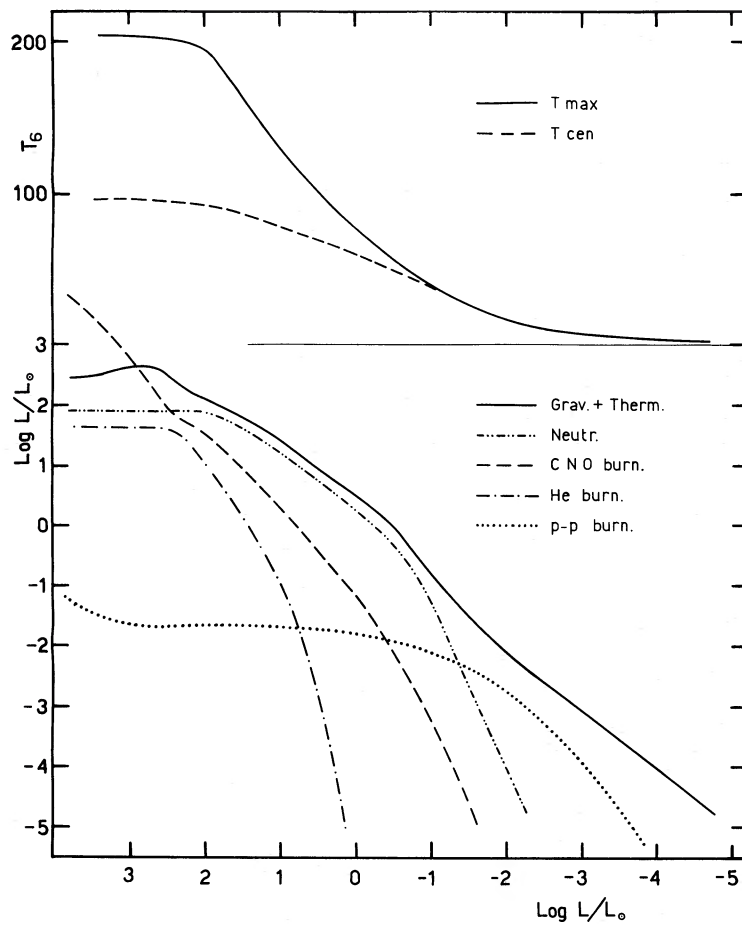


FIG. 7.—Contribution of several sources of energy in the WD sequence A, having a burning remnant hydrogen layer and metal content $Z = 0.02$ maintained along the whole evolution. The central and maximum temperature are also shown.

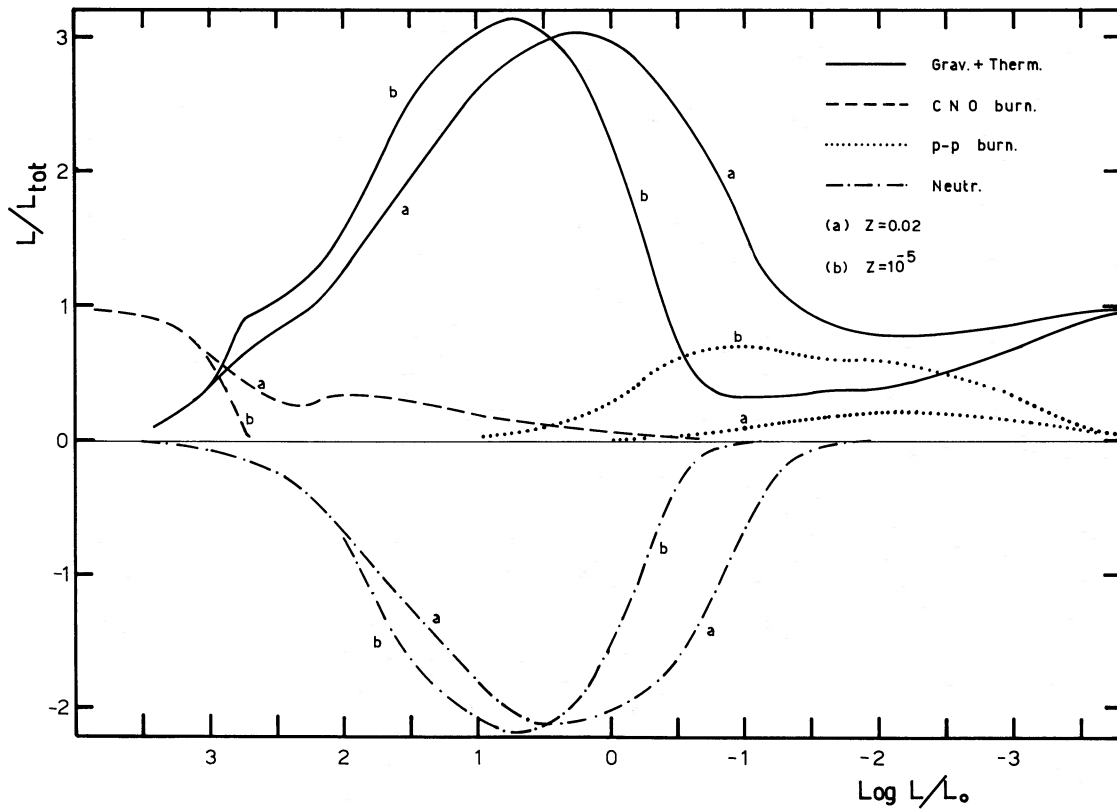


FIG. 8.—Percentages of luminosity outputs for sequences A and B. Sequence B is obtained from sequence A by artificially depleting the metal content to $Z = 10^{-5}$, at $\log L/L_{\odot} = 3.0$, as it appears from the rapid turning off of CNO energy supply. Proton-proton luminosity at $-2. < \log(L/L_{\odot}) < -1$. is considerably larger than in case A.

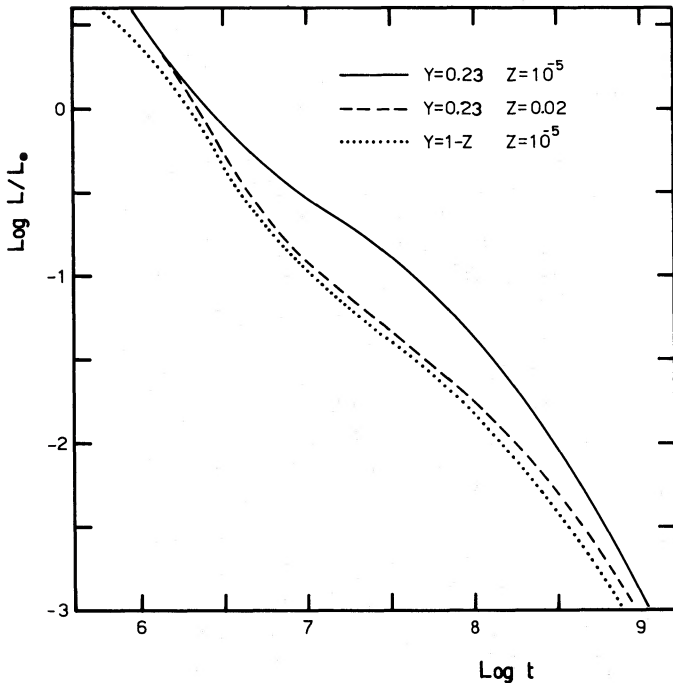


FIG. 9.—Evolutionary times for sequence A (dashed line), B (solid line), and C (dotted line) in the high-luminosity portion of WD evolution. Sequences D and E behave like sequence C. The major difference between sequence B and the others, in the range $-0.5 > \log(L/L_{\odot}) > -2.5$, is due to the large contribution of p - p burning.

hydrogen-burning, the ratio DA/non-DA should vary from 3.5 at $4.7 > \log T_{\text{eff}} > 4.45$ to 1.1 in the range $4.2 > \log T_{\text{eff}} > 4.0$, in units of the birth number ratio. If, for example, DA/non-DA = 3 at 4.2–4.0, it should be DA/non-DA = 10 at 4.7–4.45. A careful study of the luminosity function could thus confirm or provide evidence against the hypothesis that DAs retain their whole evolutionary hydrogen layer. Unfortunately, this problem cannot be addressed at present, as no non-DA is known in the range $4.65 > \log T_{\text{eff}} > 4.48$ (Wesemael, Green, and Liebert 1985)!

One more word about sequence C: since H-burning is not effective in reducing the total M_{H} to less than $10^{-4} M_{\odot}$, people have been forced to look for other removal mechanisms to reduce this value to $\sim 10^{-7} M_{\odot}$, consistent with the interpretation of the observed pulsations in DA WDs. As an example, Michaud and Fontaine (1984) have discussed the possibility of an enhanced CNO burning due to the penetration of the tail of the hydrogen distribution profile due to diffusion into the tail of the carbon diffusion-induced profile out of the core. Their helium layers are, however, at least one order of magnitude smaller than expected from evolution, and in any case Iben and McDonald (1985) have shown that this mechanism can hardly be responsible for a substantial shortage of the surface H layers. It is, however, sufficient to postulate a mass loss rate in the blue of the order of $10^{-8} M_{\odot} \text{ yr}^{-1}$, which is even smaller than those observed in these evolutionary phases, to get rid of almost all the surface hydrogen, until $M_{\text{H}} = 10^{-7} M_{\odot}$ or even less, while the surface luminosity of the star is still larger than $\log(L/L_{\odot}) \approx 2$.

c) The Crystallization Phase and the Onset of Debye Cooling

As the WD becomes less and less luminous, the thermal content release from the ions becomes the relevant source of

luminosity, and the time scale of evolution lengthens so much that the age differences built up in the previous evolutionary phases (due to the occurrence or not of nuclear burning) become less significant by the time the star reaches $\log(L/L_{\odot}) = -3.0$, at which time the WD ages range from $7.8 \times 10^8 \text{ yr}$ for sequence A to $9.2 \times 10^8 \text{ yr}$ for sequence C and to $1.2 \times 10^9 \text{ yr}$ for sequence B.

There now begins the most interesting phase in the WD life, at least from the point of view of what for a long time was called “cooling,” until IT suggested that this may be deceptive terminology. The most important physical event in the WD at $-3.2 > \log(L/L_{\odot}) > -4.0$ is the onset of crystallization.

We show in Figure 10 the behavior of internal luminosity as a function of mass fraction, for the models in sequence C during the crystallization phase. We may see a surplus of energy release which, as evolution proceeds, occurs first in the center and later in the outermost layers. In the model preceding the onset of crystallization (3470), the core luminosity output is roughly proportional to the mass fraction, as it must be for a nearly isothermal star. The model following complete crystallization (3550) indicates that by now the core luminosity output is quite small, and that 70% of the energy release comes from the outermost 30% of the WD. The final WD phases are thus dominated by the residual gravitational energy of the exterior.

In the massive hydrogen layer sequences (A and B), the progressive crystallization of the interior proceeds in the same

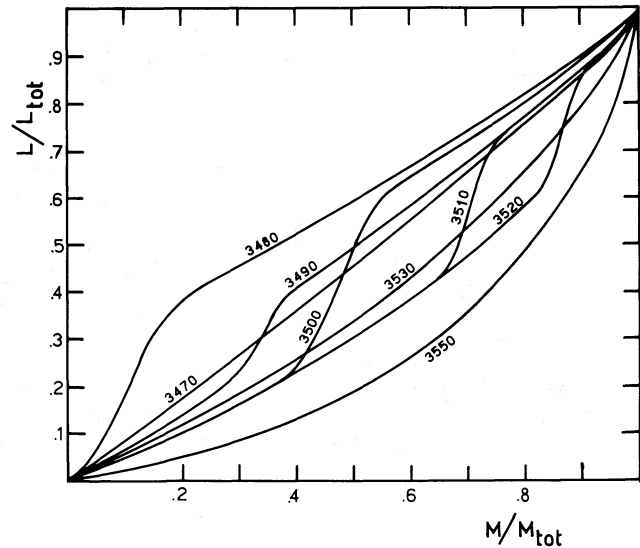


FIG. 10.—Luminosity output in the interior of the WD during the crystallization phase of sequence C. The models have the characteristics listed in Table 3.

TABLE 3
MODEL CHARACTERISTICS FOR FIGURE 10

| Model Number | $\log(L/L_{\odot})$ | $\log T_{\text{eff}}$ | $\log T_c$ | Age |
|--------------|---------------------|-----------------------|------------|------------|
| 3470.... | -3.108 | 3.948 | 6.773 | 0.92E + 09 |
| 3480.... | -3.309 | 3.898 | 6.695 | 1.28E + 09 |
| 3490.... | -3.519 | 3.846 | 6.611 | 1.85E + 09 |
| 3500.... | -3.722 | 3.796 | 6.528 | 2.50E + 09 |
| 3510.... | -3.927 | 3.745 | 6.431 | 3.52E + 09 |
| 3520.... | -4.137 | 3.693 | 6.317 | 4.78E + 09 |
| 3580.... | -4.350 | 3.639 | 6.193 | 6.02E - 09 |
| 3550.... | -4.715 | 3.544 | 5.929 | 8.15E + 09 |

qualitative fashion described in Figure 10, apart from the fact that a residual 10%–20% of the luminosity output comes from the outermost layers in which nuclear burning is still going on.

During the crystallization phase, the sequences we have computed finally differentiate: although the evolutionary times seem to finally converge, being, at $\log(L/L_\odot) = -4.0$, $t_{ev} = 3.5 \times 10^9$ yr for all the sequences, the differences which have arisen in the central temperatures will ultimately dominate the final cooling at $-4.0 > \log(L/L_\odot) > -5.0$.

In Figure 11 we show the behavior of central temperature with the luminosity: down to $\log(L/L_\odot) = -3.0$, there are negligible differences. At $-3. > \log(L/L_\odot) > -4$, in the metal-depleted helium atmosphere (sequence D), the central temperature becomes relatively smaller. In the meantime, the evolutionary times for this sequence become longer, as the star has a surplus thermal content to release, in order to attain a smaller T_c . At $\log(L/L_\odot) = -4$, $T_c = 1.4 \times 10^6$ K, compared to $T_c = 2.1 \times 10^6$ K in the sequence with $M_H = 10^{-7} M_\odot$, $Z = 10^{-5}$. The hydrogen sequence with low metals (B) begins to detach from sequence A ($Z = 0.02$) at $\log(L/L_\odot) = -3.75$. Sequence A maintains the largest T_c down to the end of the computations.

This behavior is clearly a result of the different atmospheric opacities employed, as envisioned also by IT. In the models of sequence D, having smaller opacities in the atmosphere, the photospheric pressure is much larger than in the models of sequences C and E: we are thus in the presence of a smaller temperature at any given mass point, and finally a slightly smaller T_c , in spite of the degeneracy. The situation becomes more pronounced as the luminosity reaches $\log(L/L_\odot) = -4.1$, where also the hydrogen atmosphere model of $Z = 10^{-5}$ (sequence E) has a smaller T_c than the corresponding model of sequence C.

To better clarify the role of different atmospheric opacities, we plot in figure 12 the photospheric pressure as a function of the luminosity and T_{eff} for the five sequences.

Note that (1) the hydrogen photospheric pressure has a minimum at $T_{eff} = 14,000$ K, where there is the maximum hydrogen opacity; (2) the helium sequences largely differentiate at $\log(L/L_\odot) < -2$, whereas the hydrogen sequence differentiate only at $\log(L/L_\odot) = -3.5$; the photospheric pressure is more than two orders of magnitude larger in the helium sequences than in the hydrogen ones.

Concluding, smaller atmospheric opacities produce in the end smaller central temperatures at the same luminosity. The

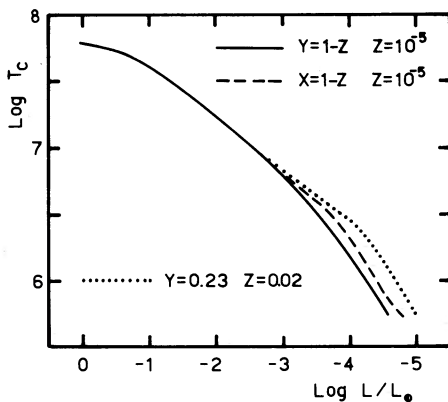


FIG. 11.—Central temperature as function of luminosity for sequences A (dotted line), B (dashed line), and D (solid line).

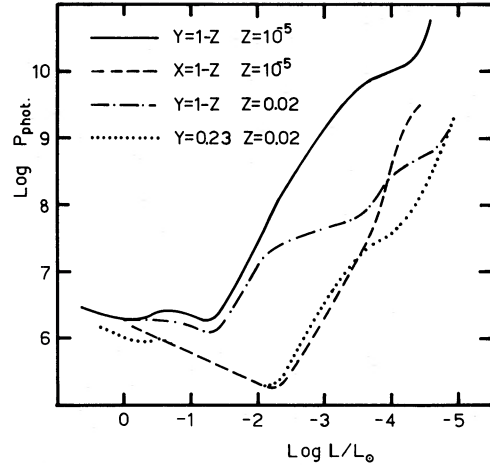


FIG. 12.—Pressure at the base of the photosphere as function of the luminosity for four sequences, indicating the role of hydrogen and metal opacities in determining the central conditions of the WD.

role of opacities is fundamental, as the corresponding thermal energy output may give a negligible lengthening of the evolutionary times, if it occurs at relatively large luminosities [$\log(L/L_\odot) > -3.5$], but the differences produced in this way may considerably affect the following evolution after the star is completely crystallized.

In Figure 13 we present the evolutionary times at the lowest luminosities for all the sequences. For the most realistic sequences D and E, the total time down to $\log(L/L_\odot) = -4.5$ is respectively 5.1×10^9 and 6.6×10^9 yr. The residual time down to invisibility cannot be longer than $\sim 1 \times 10^9$ yr for both sequences, if we adopt the formula suggested by IT.

IT find equally long ($> 10^{10}$ yr) evolutionary times for both their hydrogen and helium atmosphere sequences. They, however, stress that their low-temperature opacities may be inaccurate and predict shorter evolutionary times with smaller atmospheric opacities, just as we find.

One final consideration is due: our very short times for the helium atmosphere sequence are found at $\log(L/L_\odot) < -4.0$, where one may suspect that the physics and the opacities themselves begin to be uncertain, although real uncertainties do not intervene until $\log(L/L_\odot) \approx -4.5$, according to Magni and Mazzitelli (1979). We must stress that these times are not due to the characteristics of the models in this uncertain stage but are determined by the behavior of opacities at larger luminosities, where the overall physics is much more reliable.

TABLE 4
MIXING OF THE HYDROGEN LAYER ($M_H = 10^{-7} M_\odot$)
IN SEQUENCE E

| $\log(L/L_\odot)$ | $\log T_{eff}$ | Age | $X_H(\text{surface})$ |
|-------------------|----------------|------------|-----------------------|
| -3.8308 | 3.7684 | 2.94E + 09 | 0.99999 |
| -3.8481 | 3.7644 | 3.06E + 09 | 0.79786 |
| -3.8653 | 3.7603 | 3.20E + 09 | 0.52434 |
| -3.8840 | 3.7559 | 3.33E + 09 | 0.35161 |
| -3.9021 | 3.7514 | 3.46E + 09 | 0.35161 |
| -3.9158 | 3.7482 | 3.58E + 09 | 0.25467 |
| -3.9333 | 3.7439 | 3.71E + 09 | 0.25467 |
| -3.9630 | 3.7366 | 3.95E + 09 | 0.20548 |
| -4.2589 | 3.6618 | 5.95E + 09 | 0.20188 |
| -4.8083 | 3.5127 | 7.00E + 09 | 0.19757 |

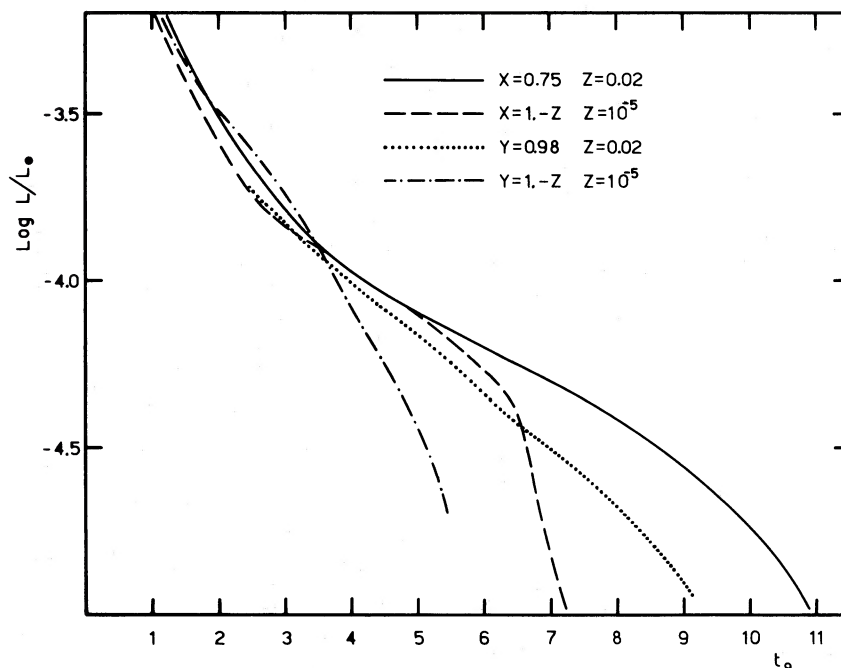


FIG. 13.—Evolutionary times at the lowest luminosities. It is to be noticed how the helium, metal-depleted sequence D (*dashed-dotted line*) spends a longer time than the others at $-4.0 < \log(L/L_{\odot}) < -3.5$, therefore being left with a smaller central temperature and heat content, when its luminosity becomes smaller than $\log(L/L_{\odot}) = -4.0$.

d) Surface Hydrogen and Convective Mixing

The H layer in sequence E was so thin ($M_{\text{H}} = 10^{-7} M_{\odot}$) that, at low enough T_{eff} , convection was effective in mixing the hydrogen layer with the underlying helium. The onset of hydrogen convection in sequence E occurred following the modalities already described in DM, thus confirming the results obtained by using only envelope models. Table 4 lists the model sequence which leads to mixing.

At $\log(L/L_{\odot}) = 3.811$, $\log T_{\text{eff}} = 3.773$, and total age $t = 9.529$, convection covered a mass $M_{\text{conv}} = 7 \times 10^{-8} M_{\odot}$, and in the following models it reached the bottom of the hydrogen layer and mixing began. The hydrogen surface abundance was reduced from $X_{\text{H}} = 0.99999$ to $X_{\text{H}} = 0.20$ in $\sim 10^9$ yr, while the luminosity went from $\log(L/L_{\odot}) = -3.83$ to -4.0 and T_{eff} from 5870 to 5450 K. From this point on, a large helium abundance was left at the surface, even if mixing of $M_{\text{H}} = 10^{-7} M_{\odot}$ of hydrogen cannot lead to an almost pure helium composition.

Consider, however, that, if most DAs suffer at least a partial mixing at low T_{eff} , as it results from the observational indications that the ratio DA/non-DAs gets smaller in the red, our evolutionary times for sequence E have to be considered as upper limits for DAs' evolutionary times. In fact, for those DAs having a thinner hydrogen layer, mixing occurs in earlier phases: for $M_{\text{H}} = 10^{-10} M_{\odot}$, for instance, we infer (DM) mixing at $\log T_{\text{eff}} = 3.88$ and almost complete H dilution in the much larger helium convective mass. We are thus left with an almost pure helium atmosphere, at $\log(L/L_{\odot}) = -3.4$, in the region where the opacity behavior may still cause the central temperature to drop to the values appropriate for the pure helium sequence and subsequently follow the evolutionary times for this latter sequence.

Thus 7×10^9 yr may be regarded as an upper limit for the evolutionary times of ordinary WDs down to $\log(L/L_{\odot}) = -5$.

VIII. CONCLUSIONS

We have followed the evolution of a $3 M_{\odot}$ Population I star from the beginning of the main sequence to the final Debye cooling as a WD, simulating the PN ejection by a very large rate of mass loss just after the first helium thermal pulse. The main conclusions one can draw from this kind of computation are, in our opinion, summarized in the following:

1. The mass of the WD coming from a $3 M_{\odot}$ star can hardly be smaller than $\sim 0.7 M_{\odot}$, unless some crucial factor is still missing from our understanding of stellar evolution.
2. The chemical composition of the WD is stratified: a core very rich in oxygen covering more than half the mass, surrounded by a carbon-rich mantle, and a helium layer of the order of $0.01\text{--}0.02 M_{\odot}$.
3. Overshooting and semiconvection can modify the final picture of point (2) very little.
4. The details of the blueward excursion in the context of the understanding of PN evolution probably have to be reinvestigated using appropriate numerical techniques, since our results indicate that the mass loss rate (and the residual helium luminosity) are also important in determining whether a visible PN will appear.
5. A mass loss rate in the blue consistent with those observed is all we need to reduce the surface hydrogen layer even to zero, without invoking mechanisms such as sedimentation-driven CNO burning.
6. The evolutionary times of WDs seem to be definitively smaller than the age of the Galactic disk, ranging between 5 and 7×10^9 yr depending on the surface chemical composition.

We thank the many people who contributed to the improvement of the presentation of these results, mainly S. Becker, A. Renzini, D. Schönberner, and V. Weidemann.

The authors' EARNET-BITNET user identification are FRANCA at IRMIAS (F. D.) and ITALO at IRMIAS (I. M.).

REFERENCES

- Alexander, D. R., Johnson, H. R., and Rypma, R. L. 1983, *Ap. J.*, **272**, 773.
 Beaudet, G., Petrosian, V., and Salpeter, E. E. 1967, *Ap. J.*, **150**, 979.
 Becker, S. A. 1981, *Ap. J. Suppl.*, **45**, 475.
 Becker, S. A., and Iben, I., Jr. 1981, *Ap. J.*, **237**, 111.
 Coleman, L. A. 1982, *A.J.*, **87**, 369.
 Cox, A. N., Starrfield, S. G., Kidman, R. B., and Pesnel, W. D., 1985, preprint.
 Cox, A. N., and Stewart, J. N. 1970, *Ap. J. Suppl.*, **19**, 243.
 D'Antona, F., and Mazzitelli, I. 1979, *Astr. Ap.*, **74**, 161 (DM).
 ———. 1986, *Astr. Ap.*, in press.
 De Zotti, G. 1972, *Mem. Soc. Astr. Italiana*, **43**, 89.
 Dolez, N., and Vauclair, G. 1981, *Astr. Ap.*, **102**, 375.
 Fontaine, G., Graboske, H. C., and Van Horn, H. M. 1977, *Ap. J. Suppl.*, **35**, 293.
 Fowler, W., Caughlan, G. R., and Zimmerman, B. A. 1975, *Ann. Rev. Astr. Ap.*, **13**, 69 (FCZ).
 Graboske, H. C., DeWitt, H. E., Grossman, H. S., and Cooper, M. S. 1973, *Ap. J.*, **181**, 457.
 Greenstein, J. L. 1986, *Ap. J.*, **304**, 334.
 Hansen, J. P. 1973, *Phys. Rev.*, **A8**, 3096.
 Harm, R., and Schwarzschild, M. 1975, *Ap. J.*, **200**, 324.
 Harris, M. J., Fowler, W. A., Caughlan, G. R., and Zimmerman, B. A. 1983, *Ann. Rev. Astr. Ap.*, **21**, 165 (HFCZ).
 Henyey, L., Vardya, M. S., and Bodenheimer, P. 1965, *Ap. J.*, **142**, 841.
 Herman, J., and Habing, H. J. 1985, *Rept. Prog. Phys. ESTEC*, in press.
 Hubbard, W. B., and Lampe, M. 1969, *Ap. J. Suppl.*, **18**, 297.
 Iben, I., Jr. 1984, *Ap. J.*, **277**, 333.
 ———. 1985, *Quart. J. R.A.S.*, **26**, 1.
 Iben, I., Jr., and McDonald, J. 1985, *Ap. J.*, **296**, 540.
 Iben, I., Jr., and Renzini, A. 1983, *Ann. Rev. Astr. Ap.*, **21**, 271.
 Iben, I. Jr., and Tutukov, A. 1984, *Ap. J.*, **282**, 615 (IT).
 Knapp, G. R., Phillips, T. G., Leighton, R. B., Lo, K. Y., Wannier, P. G., and Wotten, H. A. 1982, *Ap. J.*, **252**, 616.
 Koester, D., and Schönberner, D. 1986, *Astr. Ap.*, **154**, 125.
 Koester, D., Schulz, H., and Weidemann, V. 1979, *Astr. Ap.*, **76**, 262.
 Kutter, G. S., and Sparks, W. M. 1974, *Ap. J.*, **192**, 447.
 Lamb, D. Q., and Van Horn, H. M. 1975, *Ap. J.*, **200**, 306.
 Liebert, J. 1979, in *Colloquium 53, White Dwarfs and Variable Degenerate Stars*, ed. H. M. van Horn and V. Weidemann, (Rochester, NY: University of Rochester), p. 146.
 ———. 1980, *Ann. Rev. Astr. Ap.*, **18**, 363.
 Liebert, J., Dahn, C., Gresham, M., Hege, E. K., Moore, R. L., Romanishin, W., and Strittmatter, P. A. 1979, *Ap. J.*, **229**, 196.
 Magni, G., and Mazzitelli, I. 1979, *Astr. Ap.*, **72**, 134.
 Mazzitelli, I. 1979, *Astr. Ap.*, **79**, 251.
 ———. 1986, in preparation.
 Mazzitelli, I., and D'Antona, F. 1986, in preparation.
 Mazzitelli, I., and Moretti, M. 1980, *Ap. J.*, **235**, 955.
 Michaud, G., and Fontaine, G. 1984, *Ap. J.*, **283**, 787.
 Moss, D. L. 1986, *M.N.R.A.S.*, **152**, 47.
 Paczyński, B. 1975, *Ap. J.*, **202**, 558.
 Pollock, E. L., and Hansen, J. P. 1973, *Phys. Rev.*, **A8**, 3110.
 Reimers, D. 1975, *Mem. Soc. Roy. Sci. Liège*, 6e Sér., **8**, 369.
 Renzini, A. 1979, in *Stars and Star Systems*, ed. B. E. Westerlund (Dordrecht: Reidel), p. 409.
 ———. 1981, in *Physical Processes in Red Giants*, ed. I. Iben, Jr., and A. Renzini (Dordrecht: Reidel), p. 431.
 ———. 1984, in *IAU Symposium 103, Planetary Nebulae*, ed. D. R. Flower (Dordrecht: Reidel), p. 267.
 Schönberner, D. 1979, *Astr. Ap.*, **79**, 108.
 ———. 1981, *Astr. Ap.*, **103**, 119.
 ———. 1983, *Ap. J.*, **272**, 708.
 Schönberner, D., and Weidemann, V. 1981, in *Physical Processes in Red Giants*, ed. I. Iben and A. Renzini (Dordrecht: Reidel), p. 431.
 ———. 1982, *IAU Symposium 103, Planetary Nebulae*, ed. D. R. Flower (Dordrecht: Reidel), p. 359.
 Schwarzschild, M., and Harm, R. 1965, *Ap. J.*, **142**, 855.
 Shipman, H. L. 1979, *Ap. J.*, **228**, 240.
 Shipman, H. L., and Sass, C. 1980, *Ap. J.*, **235**, 177.
 Sion, E. M. 1979, in *IAU Colloquium 53. White Dwarfs and Variable Degenerate Stars*, ed. H. M. van Horn and V. Weidemann (Rochester, NY: University of Rochester), p. 245.
 Wehrse, R., and Liebert, J. 1980, *Astr. Ap.*, **83**, 184.
 Weidemann, V., 1975, in *Problems in Stellar Atmospheres and Envelopes*, ed. B. Baschek, W. H. Kegel, and G. Traving (Heidelberg: Springer Verlag), p. 173.
 ———. 1984, *Astr. Ap.*, **134**, L1.
 Weidemann, V., and Koester, D. 1983, *Astr. Ap.*, **121**, 77.
 Wesemael, F., Green, R., and Liebert, J. 1985, *Ap. J., Suppl.*, **58**, 379.
 Winget, D. E., Van Horn, H. M., and Hansen, C. J., 1981, *Ap. J. (Letters)*, **245**, L33.
 Zeidler-K.T., E. M. 1984, paper presented at 5th European Workshop on White Dwarfs, Kiel University.

F. D'ANTONA: Osservatorio Astronomico di Roma, I-00040 Monte Porzio, Italy

I. MAZZITELLI: Istituto di Astrofisica Spaziale del C.N.R., C.P. 67, I-00044 Frascati, Italy